S1: Expanded methods section

Input parameters for Gaussian dispersion method

The dispersion modeling described in the Methods section (main text; Equation 2) requires knowledge of the dispersion terms, σ_z and σ_y. These dispersion terms are taken from a lookup table based on a chosen Pasquill stability class and are a function of x, the downwind distance.

Pasquill stability classes define the modeled dispersion and describe the extent of spread that a simulated plume undergoes as it is transported downwind. The stability class for these results was chosen based on measured or archived meteorological data using the STAR method,(Beychok, M. R., 2005; US EPA, n.d.) as described in the SI of Yacovitch et al.(Yacovitch et al., 2015) This procedure determines the stability class based on measured wind speed, solar elevation, cloud coverage, cloud ceiling height and whether it is day or night. Six stability classes are allowed, A through D in the day and E and F at night (however, all measurements for this study were daytime measurements). These classes span conditions ranging from the least stable (most turbulent) to the most stable (least turbulent), respectively.

Wind and weather information are required for the determination of stability class and emission magnitude. Solar elevation angle was calculated from the vehicle GPS position and time. Local airport meteorological data (METAR format) was downloaded from Wunderground.com for the campaign duration. These METAR data were used to determine cloud coverage, ceiling height, and occasionally wind speed and wind direction. An anemometer mounted to the minAML boom was deployed as part of the campaign, but malfunctioned during some of the measurement times due to accumulated road dust. Therefore, the onboard wind was compared with airport winds, and the airport winds were used if there was a major disagreement between the two. For tracer release measurements, a stationary on-site anemometer was also available. Most of the dispersion calculations were "by-catch" of the tracer sites, performed in between tracer measurement periods, and so this anemometer was not in use.

Source location for Gaussian dispersion calculations

The upwind emitting well pad was manually selected on a map for each plume. The height of the emission source is fixed to 0 in all measurements. We expect this to be a decent approximation for well pads, where most of the equipment lies close to the

ground. The measurement height (sensor height) is fixed to 2.8 meters. While a plume transect may take a minute or two, the time it takes emissions to travel from the site to the measurement vehicle is often much longer. This means that the average measured wind during the transect may not correspond exactly to the average transport wind for the measured plume transect. This can lead to simulated plumes appearing spatially offset versus the measured plume. The wind bearing can be fixed to the vector between measured emission and site to mitigate this effect. This procedure can disguise plumes that are coming from neighboring or interfering sources, and so it is applied with caution.

There is an inherent degree of uncertainty to assigning emissions to a given site for Gaussian plume simulations. This is quite different from the tracer release results, where co-dispersion of methane (CH_4) with tracer allows for unambiguous assignment of a site's emissions. Figure S-1 shows an example of a somewhat ambiguous point source assignment, where three nearby inventory site locations are shown (red triangles).

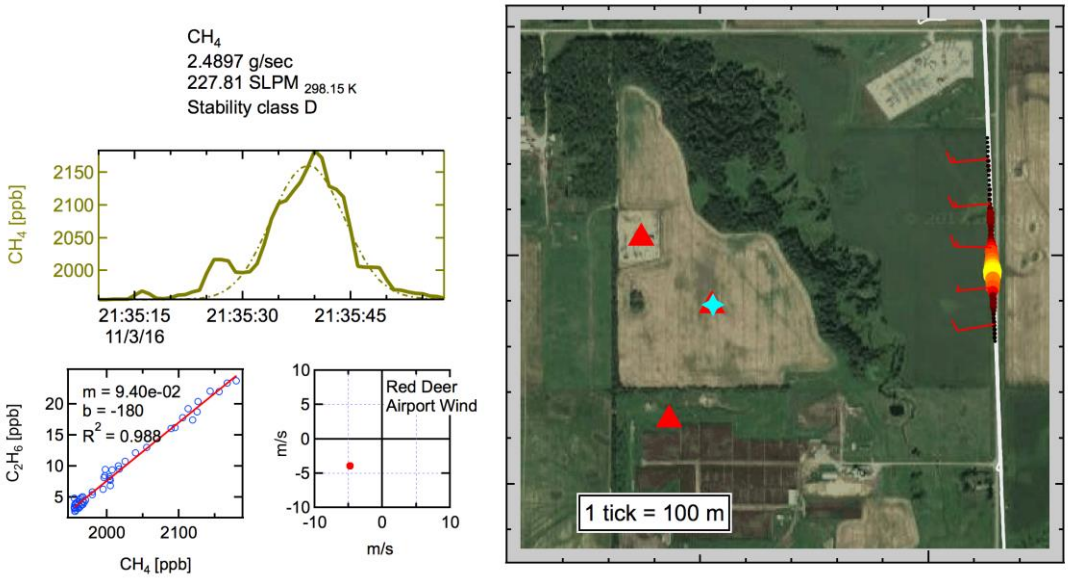

Figure S-1. Example of production site where emission source is uncertain. The well choice in a situation like this will affect both the width and shape of the simulated emission and also the final magnitude due to the difference in distances between well site and plume. Measured (solid dark yellow trace) and simulated (dotted trace) mixing ratios of CH_4 are shown (top left) along with this data's C_2H_6/ CH_4 enhancement ratio (bottom left, ratio of 11.8 %). A site map (right) shows the driven path with markers colored and sized by CH_4 enhancement (black to red to yellow). The chosen point-source for the simulation is shown (blue star) along with

inventory point sources (red triangles). Wind barbs (red arrows) point towards the site but are offset compared with nearby airport wind (bottom center).

For certain emitters, a single point source simulation cannot fully reproduce the observed CH_4 enhancements during downwind transects. One such situation arises when a close transect is done downwind of a large site with multiple distinct emission sources. Each sub-plume may be more or less distinct in the resulting transect. In these cases, a multi-source fixed release location method is used. Numerous emission sources are chosen based on inspection of a satellite map. Source locations are chosen to correspond with tank batteries, wellheads, or other distinct equipment on the map. Simulations for these facilities are performed by manually varying the relative magnitude of each point source and summing their simulated plumes in order to best reproduce the spatial structure of the measured plume.

Estimation of error for Gaussian dispersion method

There are several assumptions involved in Gaussian plume simulations and the Pasquill stability classes,(Sax, 2003; B. K. Fritz et al., 2005; Beychok, M. R., 2005; Abdel-Rahman, A. A., 2008) and thus several possible sources of systematic error in these emission flux determinations. First, no fluctuations are allowed in either the emission flux, or the average wind direction in the time it takes a plume to be emitted and reach the measurement location (~2-20 mins). Second, the stability class determination is assumed to be valid for the data in question. Third, the timescale of the measurement transect is assumed to be at the same timescale as that which the stability class parameters were developed (~3-20 mins).(B. K. Fritz et al., 2005)

The assumptions listed above can all have major effects on the results of a simulation, and thus in the determination of an emission magnitude and location based on experimental data. The question of timescales and the applicability of the concept of a stability class to transect data are of particular interest. Beychok describes the effects of different mixing ratio averaging timescales in the measured emissions,(Beychok, M. R., 2005) and Fritz et al. describe the scaling of wind measurements and associated stability classes with averaging time.(B. K. Fritz et al., 2005) These plume transects are quite different in spatial and timescale from the usual fixed sensor networks used in this type of Gaussian simulation. These questions warrant further investigation using high-frequency meteorological instruments and additional metered trace gas releases or parallel emissions determinations using Gaussian dispersion on the one hand, and tracer release on

the other,(Lamb et al., 1995; Allen et al., 2013) and are beyond the scope of this publication.

Due to the assumptions above, generous error bars are asserted for these measurements. Test data with winds ≥ 4 m/s yielded 95% confidence intervals of [0.334x, 3.34x], where x is the emission magnitude. For this study, no wind threshold was applied and factor of 10 error bars [0.1x, 10x] are asserted. These error bounds are within the range of model sensitivity analyses performed by others.(Sax, 2003; B. K. Fritz et al., 2005; Beychok, M. R., 2005; Abdel-Rahman, A. A., 2008) They can also be compared to the EPA Other Test Method 33A recently described by Brantley et al.:(Brantley et al., 2014) a Gaussian dispersion approach using stationary measurements and a custom set of atmospheric stability classes. The EPA test method was also verified using staged release data to determine errors of ±60%. These are not formal 95% confidence bounds since all data points are included, but translate roughly to errors of [0.40x, 1.6x] in the same notation as above.

Additional details about mobile laboratory

A Proton-Transfer-Reaction Mass Spectrometer (PTR-MS) was used to measure the aromatic compounds, benzene, toluene, and the sum of xylene plus ethyl benzene isomers (C_2 benzenes). The details of the mobile operation of this instrument for emission plume measurements has been previously documented.(Rogers et al., 2006; Knighton et al., 2012) The PTR-MS was operated in the H_3O^+ mode. An ambient sample taken from the common inlet was directed into the drift tube reaction region where it was exposed to a high intensity source of $H3O^+$. Any aromatic molecules that underwent a reaction with H_3O^+ were transformed into a protonated molecule, such as $C_6H_6H^+$ for benzene, which were then detected using the mass spectrometer. Benzene and toluene provide unique responses, whereas the xylenes and ethyl benzene molecules are detected as the sum of these molecules because they are isomers and cannot be differentiated by mass spectrometry. The measured mass spectral ion intensities were transformed into concentrations using calibrated response factors.

The PTR-MS was calibrated daily using a standard with ~5% uncertainties for each of the VOCs selected for quantification.

S2: Statistical estimator

We use the statistical estimator developed by Zavala-Araiza et al. (Zavala-Araiza et al., 2015) to derive the emissions probability density function (pdf) that characterizes the production sites measured during this study. The statistical estimator approach allows us to derive an integrated pdf using a systematic sample and a high-emitter biased sample of ground-based measurements. As a result, we obtain a pdf and a central estimate (site-level emission factor) that takes into account the skewedness of the collected data and the fact that a simple average of the measured sites would not consider the effect of the low probability, high-emission sites that characterize skewed distributions. The statistical estimator approach is described and justified in detail elsewhere;(Zavala-Araiza et al., 2015) here we present a small summary of the approach.

The statistical estimator is used to derive a pdf that follows a lognormal distribution (to capture the skewedness of the data). Let x be the logarithm of CH_4 emissions measured at a production site. Assuming that x is normally distributed:

$$p(x|\mu,\sigma) = \frac{1}{\sqrt{2\pi}\sigma} e^{\frac{(x-\mu)^2}{2\sigma^2}} \quad \text{(S2.1)}$$

We define $\Phi(x)$ as the cumulative standard normal:

$$\Phi(x) = \int_{-\infty}^{x} \frac{1}{\sqrt{2\pi}} e^{-\frac{\vartheta^2}{2}} d\vartheta \quad \text{(S2.2)}$$

And:

$$\int_{-\infty}^{x} p(\vartheta|\mu,\sigma)\, d\vartheta = \Phi\left(\frac{x-\mu}{\sigma}\right) \quad \text{(S2.3)}$$

The log-likelihood function that describes a random or systematic sample is:

$$l_{sistematic}(\mu,\sigma) = S_0 ln\, \Phi\left(\frac{x^*-\mu}{\sigma}\right) - S_r ln\sigma - \sum_{i=1}^{S_r} \frac{(x_i-\mu)^2}{2\sigma^2} \quad \text{(S2.4)}$$

where x^*, is the detection limit for the production sites measurements, S_0[1] is the number of measurements at or below the detection limit and S_r is the number of measurements above the detection limit.

As described in detail in Zavala-Araiza et al.(Zavala-Araiza et al., 2015), for the case of an additional dataset of higher-emitter biased samples, we use the notion

[1] For this work, no measurements were classified as below the detection limit, thus $S_o = 0$. See Section S3.

that larger sources can be detected further downwind than smaller sources — which makes their search area larger. In other words, the sampled area grows with emissions: $A(E)$.

Let $q(x)$ be the probability density of the log of the emissions for the biased samples,

$$q(x) = \frac{A(x)\frac{1}{\sqrt{2\pi}\sigma}e^{-\frac{(x-\mu)^2}{2\sigma^2}}}{\int_0^\infty A(x)\frac{1}{\sqrt{2\pi}\sigma}e^{-\frac{(v-\mu)^2}{2\sigma^2}}dv} \tag{S2.5}$$

We model the high-emitter bias dependency as a power law:

$$A(E) = cE^\theta \tag{S2.6}$$

Or

$$A(x) = ce^{x\theta} \tag{S2.7}$$

Combining equation S2.5 and S2.7 and completing the square:

$$q(x) = \frac{1}{\sqrt{2\pi}\sigma}e^{-\frac{(x-\mu-\theta\sigma^2)^2}{2\sigma^2}} \tag{S2.8}$$

Thus, following the assumption that the systematic samples follow a lognormal distribution, the high-emitter biased samples is described by a lognormal distribution with mean $\mu + \theta\sigma^2$.

The log-likelihood function that describes the high-emitter biased sample is:

$$l_{high}(\mu, \sigma, \theta) = -S_h ln\sigma + \sum_{j=1}^{S_h}\frac{(x_j-\mu-\theta\sigma^2)^2}{2\sigma^2} \tag{S2.9}$$

where S_h is the number of high-emitter biased samples.

We run an optimization routine to estimate μ, σ, θ from equations S2.4 and S2.9. This is done in two ways:

(i) Using solely the systematic sample (i.e., data collected using the tracer flux method). In this case, the maximum likelihood estimate is only from equation S2.4.

(ii) Using the systematic sample and then adding the high-emitter bias samples (i.e., data collected using the Gaussian dispersion method). In this case, the maximum likelihood estimate is from the sum of equations S2.4 and S2.9.

From the maximum likelihood estimated parameters it is possible to derive a central, site-level emission factor, EF:

$$EF = e^{\mu+\frac{1}{2\sigma^2}} \quad \text{(S2.10)}$$

We summarize the results of both variations of the statistical estimator in Table S-1. Zavala-Araiza et al.(Zavala-Araiza et al., 2015) provide an extensive discussion of estimation of uncertainty as well as additional variations to the methods that test the applicability of the statistical estimator to site-level emission rates from downwind measurements.

Table S-1. Summary of parameters from the statistical estimator. The 95% confidence intervals (CI) are shown between parentheses.

Variation of the statistical estimator	$\boldsymbol{\mu}$	$\boldsymbol{\sigma}$	$\boldsymbol{\theta}$	$\boldsymbol{EF}$ **(kg CH_4 h^{-1})**
Systematic sample only (tracer flux method)	-0.31 (-0.89, 0.27)	1.5 (1.1, 1.9)	—	2.2 (1.0, 5.4)
Systematic sample + high-emitter bias sample (tracer flux + Gaussian dispersion method)	-0.31 (-0.96, 0.34)	1.7 (1.4, 2.0)	0.40 (0.061, 0.74)	2.9 (1.3, 6.8)

When we integrate the systematic samples and the high-emitter biased samples we get an EF with a central estimate that is 33% higher than the one produced when we only use the systematic sample. In Zavala-Araiza et al. (Zavala-Araiza et al., 2015) the two methods were applied to measurements of production sites in the Barnett Shale (Texas, US), producing the same result (difference < 3%). This could be explained by the significantly higher number of measurements utilized in Zavala-Araiza et al.: The systematic sample included 186 measurements (production sites only) plus 81 measurements from the high-emitter biased sample.

The difference between the two variations in the statistical estimator is likely driven by the small sample size of the systematic sample in this work. We would

expect that as the size of the systematic sample increases, the results from both variations would converge into the same pdf. As a consequence, we present the results from both variations (Figure S2).

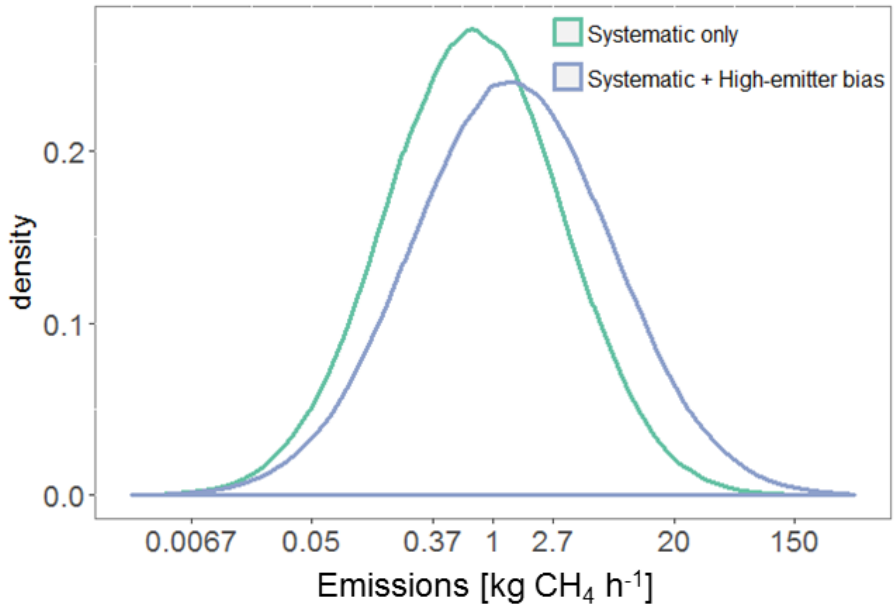

Figure S-2. Fitted pdf under both variations of the statistical estimator.

We use the Kolmogorov-Smirnov test to assess if our sampled distribution (systematic sample) is accurately described by a lognormal distribution. For a p-value of 0.751 (significance level = 0.05) we accept the null hypothesis stating that the sampled data follows the proposed lognormal distribution.

S3: Characteristics of measured sites

Table S-2. Summary of characteristics from production sites measured in this work. The table splits the measurements based on the measurement method used and also shows a combined total. The final column in the table compares the sampled population with the population of production sites within the bounding box of Figure 1 (main text).

Method	Tracer flux (systematic sample)	Gaussian dispersion (high-emitter biased sample)	Combined total	Production sites in Figure 1 (*main text*)
Number of production sites	25	35	60	11,000
Number of wells per site	*Mean*: 1.1 *Median:* 1.0 *Range*: [1 – 2]	*Mean*: 1.2 *Median:* 1.0 *Range*: [1 – 3]	*Mean*: 1.2 *Median:* 1.0 *Range*: [1 – 3]	*Mean*: 1.2 *Median:* 1.0 *Range*: [1 – 7]
Age of wells (years)	*Mean*: 22 *Median:* 19 *Range* [4.10 – 54]	*Mean*: 17 Median: 15 *Range*: [0.2 – 51]	*Mean*: 19 *Median:* 17 *Range*: [0.2 – 54]	*Mean*: 15 *Median:* 11 *Range*: [0.08 – 55]
Gas production (Mcf d^{-1})	*Mean*: 72 *Median:* 32 *Range*: [0 – 230]	*Mean*: 150 *Median:* 93 *Range*: [0 – 660]	*Mean*: 120 *Median:* 57 *Range*: [0 – 660]	*Mean*: 98 *Median:* 43 *Range*: [0 – 13,000]
Oil production (bbl d^{-1})	*Mean*: 0.80 *Median:* 0.0 *Range*: [0 – 8.4]	*Mean*: 22 *Median:* 0.067 *Range*: [0 – 440]	*Mean*: 13 *Median:* 0.0 *Range*: [0.0 – 440]	*Mean*: 3.4 *Median:* 0.0 *Range*: [0.0 – 1,800]

S4: Multiple regression analysis

We tested multiple regression models with different combinations of production site parameters as predictors for emissions. The selected model had the lowest Akaike information criterion (AIC) value, and the inclusion of each additional predictor was statistically significant. Equation S5.1 describes the final model and Table S3 summarizes the parameters in the model.

$$Emissions_{CH_4} = \beta_1(gas\ production) + \beta_2(oil\ production) + \beta_3(age) + \beta_4\{(gas\ production) \times (age)\} \pm \epsilon \quad \text{(S4.1)}$$

where $Emissions_{CH_4}$ are in $[kg\ CH_4\ h^{-1}]$, gas production in $[Mcf d^{-1}]$, oil production in $[bbl\ d^{-1}]$, age in years, and ϵ is the residual standard error term.

Table S-3. Summary of multiple regression model parameters. Even though some predictors have an individual p-value > 0.05, their presence in the model is statistically significant ($p < 1 \times 10^{-4}$). This model has an adjusted R^2 of 0.640 and ϵ of 2.04.

Predictor	Coefficient	Std. Error	p value
gas production, $\boldsymbol{\beta_1}$	-0.00236	0.0103	0.821
oil production, $\boldsymbol{\beta_2}$	0.466	0.229	0.0552
age, $\boldsymbol{\beta_3}$	-0.00195	0.0196	0.922
gas production : age, $\boldsymbol{\beta_4}$	0.00104	0.00041	0.0188

To illustrate this behavior we used our regression model to estimate emissions for a range of gas production volumes under different assumed ages and fixed oil production (Figure S-3). We see a higher increase in emissions (steeper positive slope) as we transition to older sites. This could be explained by the fact that older sites are more prone to situations that could cause excess emissions (e.g., malfunctions, failures, older equipment).

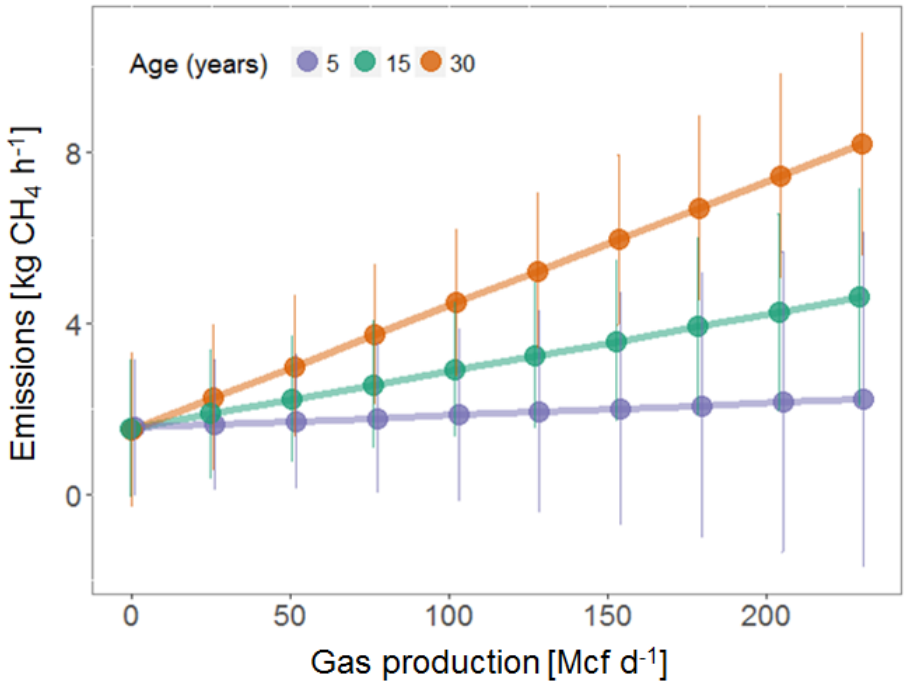

Figure S-3. Multiple regression analysis results. The plot shows the impact of the interaction term between well age and gas production in our regression model. As illustrated by the changing slope of the lines, gas production has an increasingly higher effect on emissions as sites get older. The plot shows a fixed oil production at 3.4 bbl d^{-1}, however, a higher/lower oil production would displace the lines to higher/lower emissions without affecting the slopes. We show the 95% confidence intervals of the regression model as vertical lines.

S5: Comparing ground-based measurements to airborne-based measurements

Johnson et al. report regional CH_4 and C_2H_6 emission rates based on airborne measurements from a series of flights conducted between October 27 – November 5, 2016.(Johnson et al., 2017) Figure S-4 shows the location of the 50 km x 50 km region that was sampled by the aircraft as well as the ground-based measurements reported in this work.

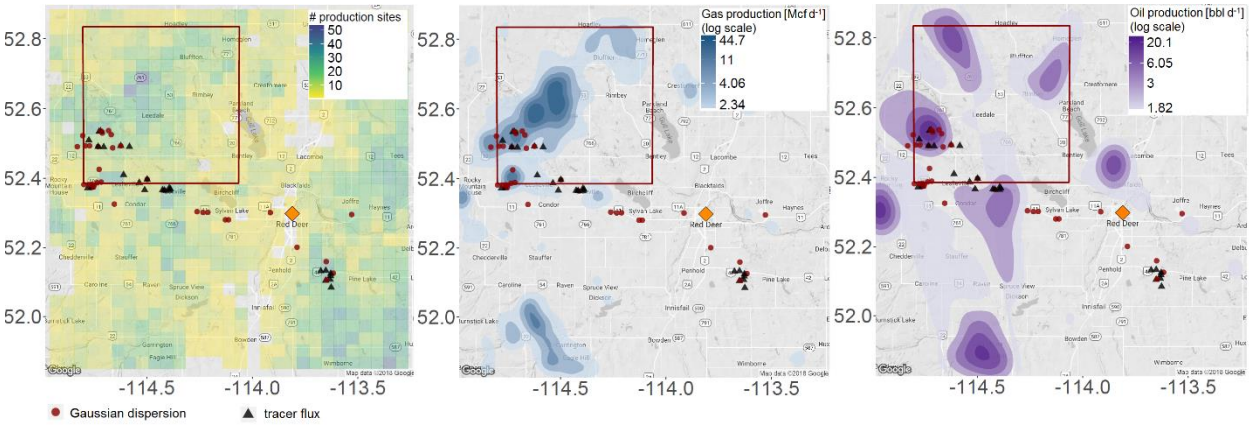

Figure S-4. Study region, ground-based and airborne-based measurements. Maps illustrating location of measured oil and gas production sites as well as 50 km x 50 km box (red box) where Johnson et al. performed airborne-based regional estimate of emissions.(Johnson et al., 2017) Measurements using the tracer flux method are shown as dark grey triangles while measurements using Gaussian dispersion method are shown as red dots. Left: density of natural gas production sites. Middle and right: contour plots illustrating hotspots for gas production and oil production, respectively.

Figure S-5 shows the cdfs comparing gas production from gas sites from the samples and gas sites within the 50 km x 50 km box, illustrating that gas production is very similar: mean gas production is 150 Mcf d^{-1} (4.1 × 1000 m^3 d^{-1}) and 160 Mcf d^{-1} (4.6 × 1000 m^3 d^{-1}) for the samples and the population, respectively. For sites classified as oil sites the mean gas to oil ratio (GOR) is also very similar: 2,800 m^3/m^3 and 2,600 m^3/m^3 for the samples and the population, respectively.

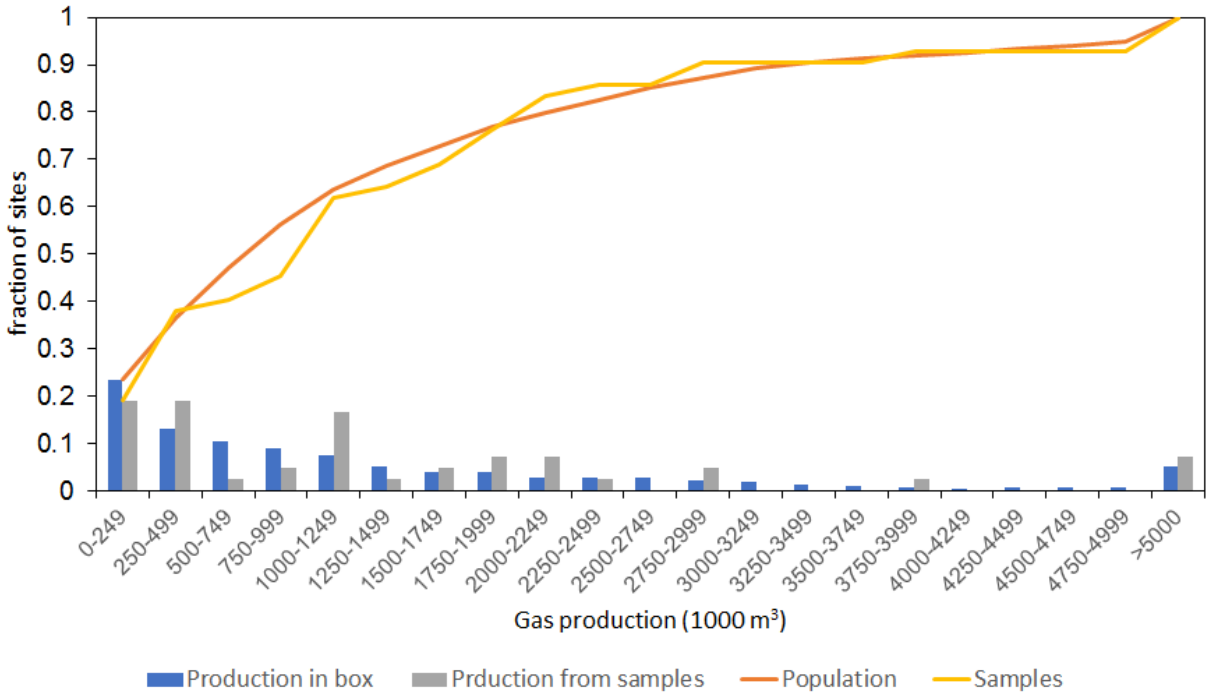

Figure S-5. Distribution of gas production from sites in the study region. CDF plot comparing gas production distribution of samples and sites within the 50 km x 50 km box where Johnson et al. performed airborne-based regional estimate of emissions (Johnson et al., 2017) (for sites classified as gas sites).

S6: Relationship between emission rates and produced gas

We replicate the analysis reported in Zavala-Araiza et al.,(Zavala-Araiza et al., 2015) where a pdf of proportional loss rates (CH_4 emissions normalized by CH_4 production) is derived from the joint density of CH_4 emissions and production. Details about the analysis are provided in Zavala-Araiza et al.; here we summarize the methods.

Let x be the logarithm of CH_4 emissions measured at a production site, y the logarithm of total CH_4 production at a production site, and z the logarithm of the proportional loss rate (CH_4 emissions normalized by CH_4 production). We use the systematic sample to estimate the pdf of emissions conditional on production $P(x|y)$, with parameters μ_x, σ_x, where μ_x is expressed as a linear regression of production:

$$\mu_x = A + By \tag{S6.1}$$

In a similar way, we estimate the pdf of y, with parameters μ_y, σ_y, assuming that y is also normally distributed and applying equations S2.1 – S2.4. Since both x and y are normally distributed we can compute the joint density $D(x, y)$ as a bivariate normal distribution (Figure S-6).

We can express the relationship between the logarithms of proportional loss rate, emissions, and production as:

$$z = x - y \tag{S6.2}$$

Thus, we can express y as a function of x and z, express the joint density $D(x, z)$, and finally compute the marginal probability of proportional loss rates $P(z)$ as:

$$P(z) = \int_{-\infty}^{\infty} D(x, z)dx \tag{S6.3}$$

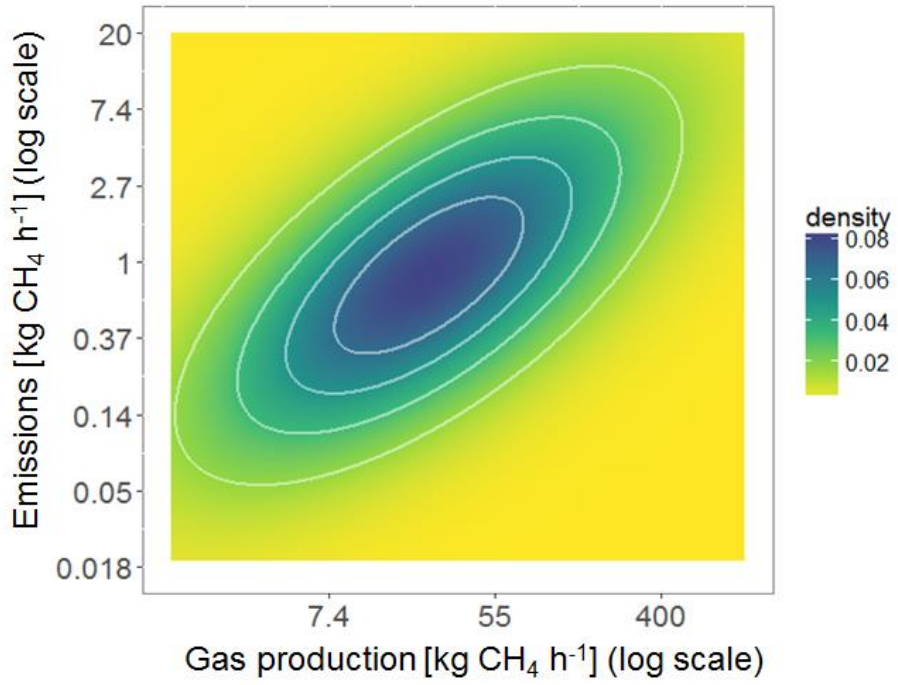

Figure S-6. Contour plot of the joint density of emission rates and production.

S7: Deriving emission distributions for other North American production regions

In order to contextualize our results, we compare our estimates to measurements performed with similar approaches (ground-based, downwind characterization of site-level emissions of production sites) in different oil and gas production regions within the US: Barnett Shale, Texas;(Rella et al., 2015; Zavala-Araiza et al., 2015) Denver-Julesburg, Colorado;(Brantley et al., 2014; Robertson et al., 2017) Fayetteville, Arkansas;(Robertson et al., 2017) Marcellus Shale, Pennsylvania and West Virginia;(Omara et al., 2016) Uintah, Utah;(Robertson et al., 2017) and Upper Green River, Wyoming.(Robertson et al., 2017)

All of these studies reported systematic samples of production sites. However, every one of them relied on a different method to estimate a central emission factor. As a consequence, we extract the datasets of production site emission rates reported for each region (Figure S-7) and replicate the statistical estimator method described earlier in this work (Section S2). As a result, for each production region we produce a pdf of emissions (Figure S-8) and we also analyze the relationship of emissions and production (replicating the analysis shown in Section S7).

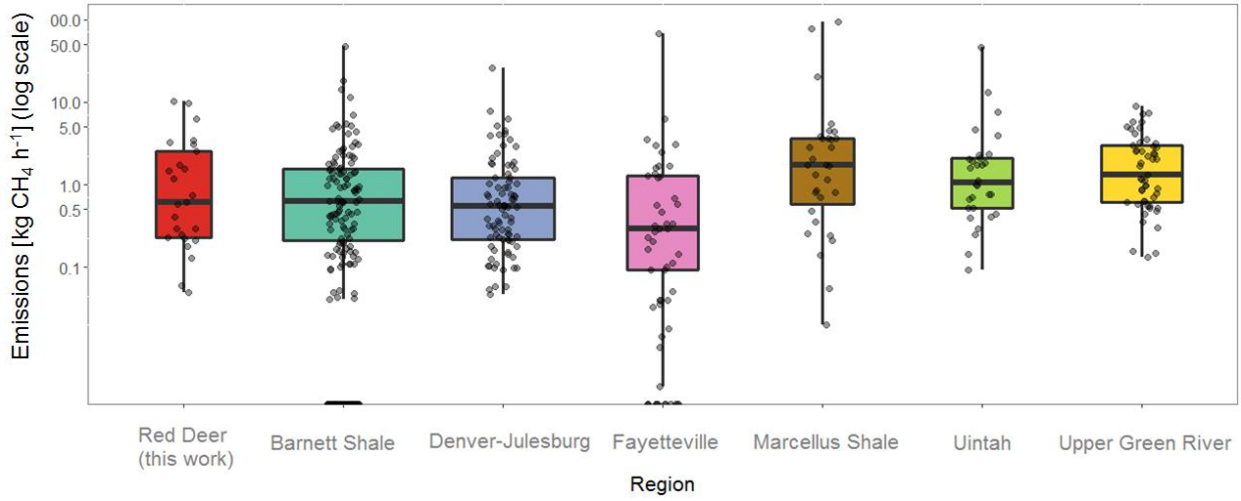

Figure S-7. Emissions per production region. For each region, boxplots show distribution of sampled datasets. The horizontal line at the middle of each box represents the median; the vertical bounds of the boxes show the 25th and 75th percentiles. The width of the boxes represents the relative sample size for each method. The maximum and minimum values are represented by the length of the whiskers. The data points (with jitter) are overlaid on top of the boxplots. Data points at the bottom of the boxplots represent censored data (below the detection limit).

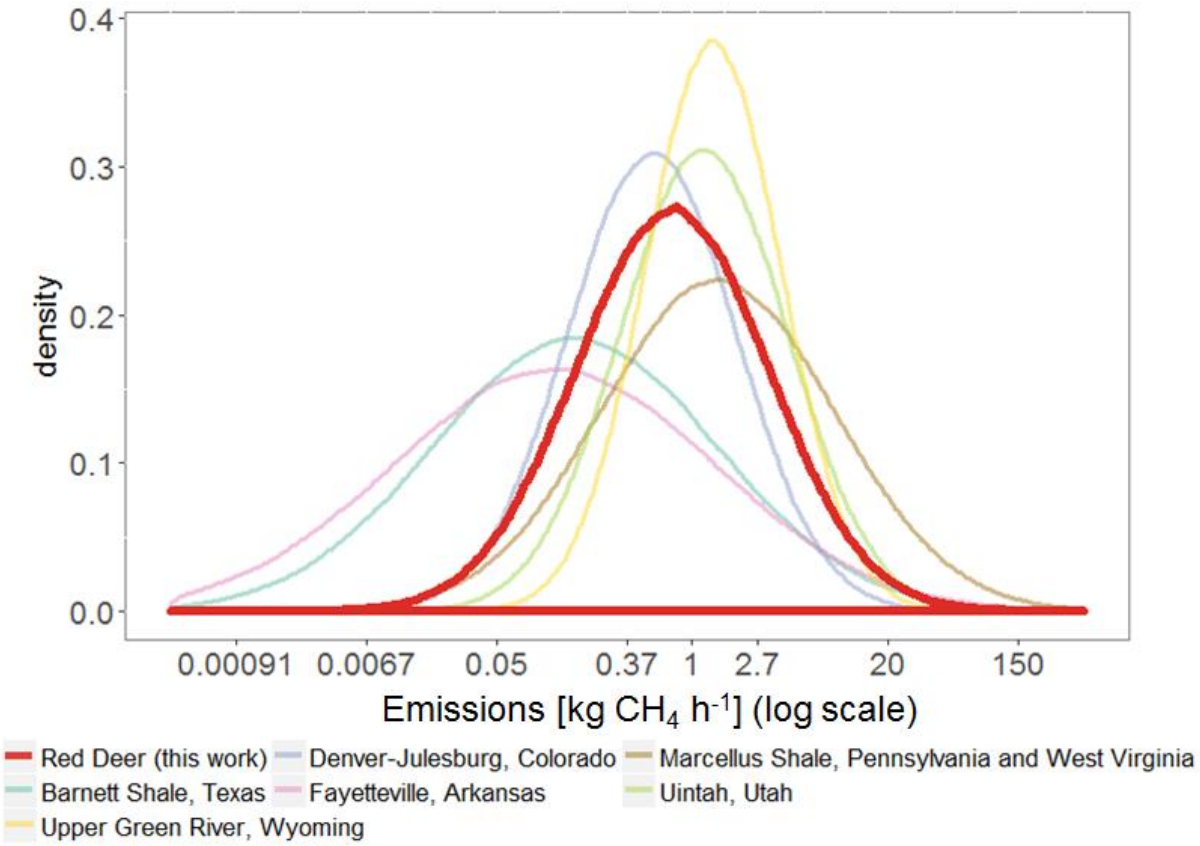

Figure S-8. For each region, fitted pdf under the statistical estimator.

Table S-4 summarizes the pdf parameters and central estimates for each of the production regions. For each case, we performed the Kolmogorov-Smirnov test or the Quadratic Class Upper Tail Anderson-Darling statistic (in the case of datasets with censored data)(Chernobai et al., 2005) to assess if our sampled distributions (systematic samples) were accurately described by a lognormal distribution. In all cases we conclude that the lognormal distribution is an accurate characterization of the sampled distributions.

Table S-4. Summary of parameters for each of the production regions that we used in our comparison. The 95% confidence interval (CI) is shown between parentheses.

Region	Study	Fitted pdf parameters	EF (kg CH_4 h^{-1})	Median proportional loss rate (%)
Red Deer	This work	μ = -0.31 (-0.89, 0.27) σ = 1.5 (1.1, 1.9) N = 25	2.2 (1.0, 5.4)	3.3%
Barnett Shale, Texas	Zavala-Araiza et al.(Zavala-Araiza et al., 2015)*	μ = -1.8 (-2.1, -1.5) σ = 2.2 (2.0, 2.4) N = 186	1.8 (1.3, 2.5)	0.31%
Denver-Julesburg, Colorado	Robertson et al.(Robertson et al., 2017)**	μ = -0.62 (-0.9, -0.34) σ = 1.3 (1.1, 1.5) N = 84	1.2 (0.87, 1.8)	1.8%
Fayetteville, Arkansas	Robertson et al.(Robertson et al., 2017)	μ = -2.1 (-2.8, -1.4) σ = 2.5 (1.9, 3.1) N = 53	2.5 (0.55, 16)	0.036%
Marcellus Shale, Pennsylvania and West Virginia	Omara et al. (Omara et al., 2016)***	μ = 0.39 (-0.24, 1.0) σ = 1.8 (1.3, 2.2) N = 31	7.3 (2.9, 21)	1.6%
Uintah, Utah	Robertson et al.(Robertson et al., 2017)	μ = 0.17 (-0.28,0.63) σ = 1.3 (0.96, 1.6) N = 30	2.7 (1.5, 5.1)	2.7%
Upper Green River, Wyoming	Robertson et al.(Robertson et al., 2017)	μ = 0.32 (0.031,0.60) σ = 1.0 (0.84, 1.2) N = 51	2.4 (1.7, 3.4)	0.37%

* Zavala-Araiza et al. reported the statistical estimator, using measurements reported originally by Rella et al.(Rella et al., 2015)

**For this region, Robertson et al. included additional measurements previously reported by Brantley et al.(Brantley et al., 2014)

***Four samples were not considered in this analysis because the sites had completion events during the time of the measurements.(Omara et al., 2016)

REFERENCES

Abdel-Rahman, A. A. 2008. On the dispersion models and atmospheric dispersion. 2008. 2nd International Conference on Waste Management, Water Pollution, Air Pollution, Indoor Climate; Corfu, Greece. WSEAS Press.

Allen DT, Torres VM, Thomas J, Sullivan DW, Harrison M, Hendler A, Herndon SC, Kolb CE, Fraser MP, Hill AD, et al. 2013. Measurements of methane emissions at natural gas production sites in the United States. *Proc Natl Acad Sci* **110**(44): 17768–17773.

B. K. Fritz, B. W. Shaw, C. B. Parnell, Jr. 2005. Influence of meteorological time frame and variation on horizontal dispersion coefficients in Gaussian dispersion modeling. *Trans ASAE* **48**(3): 1185–1196. doi: 10.13031/2013.18501

Beychok, M. R. 2005. *Fundamentals of stack gas dispersion*. 4th ed. Irvine, CA.: published by author.

Brantley HL, Thoma ED, Squier WC, Guven BB, Lyon D. 2014. Assessment of methane emissions from oil and gas production pads using mobile measurements. *Environ Sci Technol* **48**(24): 14508–14515. doi: 10.1021/es503070q

Chernobai A, Rachev S, Fabozzi F. 2005. Composite goodness-of-fit tests for left-truncated loss samples. *Dep Stat Appl Probab Univ Calif St Barbara*, in press. Available at https://statistik.econ.kit.edu/download/doc_secure1/tr_composite_goodness_tests.pdf. Accessed 2017 Jul 7.

Johnson MR, Tyner DR, Conley S, Schwietzke S, Zavala-Araiza D. 2017. Comparisons of airborne measurements and inventory estimates of methane emissions in the Alberta upstream oil and gas sector. *Environ Sci Technol* **51**(21): 13008-13017. . doi: 10.1021/acs.est.7b03525

Knighton WB, Herndon SC, Franklin JF, Wood EC, Wormhoudt J, Brooks W, Fortner EC, Allen DT. 2012. Direct measurement of volatile organic compound emissions from industrial flares using real-time online techniques: proton transfer reaction mass spectrometry and tunable infrared laser differential absorption spectroscopy. *Ind Eng Chem Res* **51**(39): 12674–12684.

Lamb BK, McManus JB, Shorter JH, Kolb CE, Mosher B, Harriss RC, Allwine E, Blaha D, Howard T, Guenther A, et al. 1995. Development of atmospheric tracer methods to measure methane emissions from natural gas facilities and urban areas. *Environ Sci Technol* **29**(6): 1468–1479.

Omara M, Sullivan MR, Li X, Subramanian R, Robinson AL, Presto AA. 2016 Jan 29. Methane emissions from conventional and unconventional natural gas production sites in the Marcellus Shale Basin. *Environ Sci Technol*, in press. doi: 10.1021/acs.est.5b05503

Rella CW, Tsai TR, Botkin CG, Crosson ER, Steele D. 2015. Measuring emissions from oil and natural gas well pads using the mobile flux plane technique. *Environ Sci Technol* **49**(7): 4742–4748. doi: 10.1021/acs.est.5b00099

Robertson AM, Edie R, Snare D, Soltis J, Field RA, Burkhart MD, Bell CS, Zimmerle D, Murphy SM. 2017 Jun 19. Variation in methane emission rates from well pads in four oil and gas basins with contrasting production volumes and compositions. *Environ Sci Technol*, in press. doi: 10.1021/acs.est.7b00571

Rogers TM, Grimsrud EP, Herndon SC, Jayne JT, Kolb CE, Allwine E, Westberg H, Lamb BK, Zavala M, Molina LT, et al. 2006. On-road measurements of volatile organic compounds in the Mexico City metropolitan area using proton transfer reaction mass spectrometry. *Int J Mass Spectrom* **252**(1): 26–37.

Sax T. 2003. A case study for assessing uncertainty in local-scale regulatory air quality modeling applications. *Atmos Environ* **37**(25): 3481–3489. doi: 10.1016/S1352-2310(03)00411-4

US EPA. n.d. STAR (STability ARray program), in meteorological processors and accessory programs. Meteorological processors and accessory programs. Available at https://www.epa.gov/scram/meteorological-processors-and-accessory-programs#star. Accessed 2017 Jun 15.

Yacovitch TI, Herndon SC, Pétron G, Kofler J, Lyon D, Zahniser MS, Kolb CE. 2015. Mobile laboratory observations of methane emissions in the Barnett Shale Region. *Environ Sci Technol* **49**(13): 7889–7895. doi: 10.1021/es506352j

Zavala-Araiza D, Lyon DR, Alvarez RA, Davis KJ, Harriss R, Herndon SC, Karion A, Kort EA, Lamb BK, Lan X, et al. 2015. Reconciling divergent estimates of oil and gas methane emissions. *Proc Natl Acad Sci* **112**(51): 15597–15602. doi: 10.1073/pnas.1522126112